Journal of Marine Science and Technology

Volume 25 | Issue 2 Article 19

STUDY OF JUNCTION FLOW STRUCTURES WITH DIFFERENT TURBULENCE MODELS

Jun Pei Lee
Department of Systems Engineering and Naval Architecture, National Taiwan Ocean University, Keelung, Taiwan, R.O.C.

Jiahn-Horng Chen
Department of Systems Engineering and Naval Architecture, National Taiwan Ocean University, Keelung, Taiwan, R.O.C., b0105@mail.ntou.edu.tw

Ching-Yeh Hsin
Department of Systems Engineering and Naval Architecture, National Taiwan Ocean University, Keelung, Taiwan, R.O.C.

Journal of Marine Science and Technology, Vol. 25, No. 2, pp. 178-185 (2017)
DOI: 10.6119/JMST-016-1116-2

STUDY OF JUNCTION FLOW STRUCTURES WITH DIFFERENT TURBULENCE MODELS

Jun Pei Lee, Jiahn-Horng Chen, and Ching-Yeh Hsin

Key words: junction flow, turbulence model, horseshoe vortex, flow separation.

ABSTRACT

In the present study, we conducted a series of computations to investigate the effects of turbulence models on the the development of horseshoe vortices for flow past a finite wing mounted on a flat plate. The cross section of the wing is a combination of a semi-ellipse at the nose and a NACA0020 airfoil at the tail which join each other at the location of maximum thickness. The Reynolds number is 5×10^5, based on the chord length of the wing, c. The maximum thickness is $0.235c$ and the span of the wing is $0.75c$. Both the linear and nonlinear models were employed. The former include Spalart-Allmaras model (1-equation model), standard k-ε model, realizable k-ε model, and SST k-ω model (2-equation models) and the latter are the $V2$-f model and the Reynolds stress model. The results show that different models may lead to significantly different numerical solutions. While some of them are closer to the experimental data, the others differ quite significantly.

I. INTRODUCTION

Junction flows are complicated three-dimensional flows. They are resulted from flow separation when a boundary layer passes an obstacle mounted on the same surface. Physically, the separation is due to the pressure gradients around the obstacle and induces highly unsteady horseshoe vortices resulting in high turbulence intensities and surface pressure fluctuations. Junction flows are common in engineering applications. The flows around small parts on a circuit board of computer, junctions in turbomachinery, junctions of tall buildings rising on the ground, wing-body junctions on aircraft, and control surfaces on ship and submarine hulls are just some important examples.

Simpson (2001) reviewed the typical physical features of some pratical laminar and turbulent junction flows around bluff and streamlined obstacles. He discussed effects of various geometrical parameters and elucidated their physical significances. Moreover, many studies have been conducted experimentally and computationally to reveal flow physics. Dickinson (1986a, 1986b) conducted a series of flow visualizations, pressure measurements, and three dimensional mean and fluctuating velocity measurements for appendage-flat plate junction flow with a turbulent incoming boundary layer. Fleming et al. (1993) focused on the effects of the approaching boundary layer characteristics on the junction flow. They found that the "momentum deficit factor" directly affected the mean junction flow characteristics. Baker (1979) showed that as the Reynolds number increased, the flow topology changed from a single steady primary horseshoe vortex to steady multiple vortices for laminar junction flows. The experiments by Pierce and Shin (1992) reveal a drifting single large dominant vortex and a very small corner vortex for a turbulent junction flow formed by a streamlined cylinder. The studies in the literature have shown that the junction flow is strongly dependent on the Reynolds number, obstacle geometry, and incoming flow quality.

In addition to experiment, computation is also an important tool to capture the junction flow physics. Significant amounts of modeling work have been available in the literature. Most studies are based on the Eulerian model. To take turbulence into proper consideration, most work has been conducted using the Reynolds-averaged Navier-Stokes (RANS) equations in computations. Deng and Piquet (1992) gave a comprehensive review of the early development on numerical treatment of horseshoe-vortex processes. It is well known that in the approach with the RANS equations, a turbulence model must be employed to close the equation systems. Therefore, the choice of turbulence models plays a central role in the simulation. Apsley and Leschziner (2001) computationally studied 12 turbulence models for flow past a generic wing-body junction. The geometry of the wing consists of a 3:2 semi-elliptic nose (with its major axis aligned with the approach flow) and a NACA0020-section tail. The wing is mounted on a flat plate with the oncoming stream with a zero angle of attack. Focusing on the structure of the horseshoe vortex and its effects on the forward flow, they concluded that the second-moment closure offered predictive advantages over the other models. However, they also found that no model achieved close agreement with the experimental data in respect of both mean flow and turbulence quantities.

Recently, large eddy simulation (LES) has been employed

Paper submitted 06/25/16; revised 08/02/16; accepted 11/16/16. Author for correspondence: Jiahn-Horng Chen (e-mail: b0105@mail.ntou.edu.tw).
Department of Systems Engineering and Naval Architecture, National Taiwan Ocean University, Keelung, Taiwan, R.O.C.

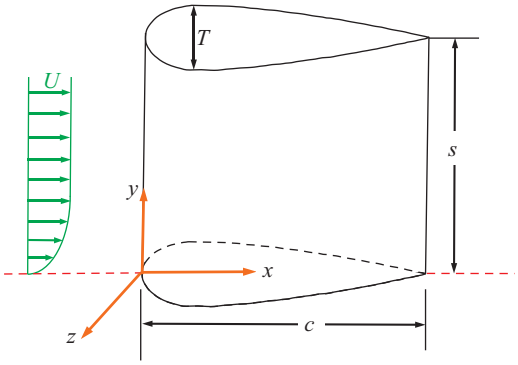

Fig. 1. Schematic of the junction flow.

to simulate the large-scale unsteady vortex structures along the body mounted on the plane. Fu et al. (2007) developed a RANS/LES hybrid method for flows passing a wing-body junction at a non-zero angle of attack. The core idea of the method is to combine RANS near the wall with LES in the separation region. Wong and Png (2009) compared different LES models and found that all models were able to capture the main physics of the highly strained, anisotropic, and unsteady flow. However, significant differences in the numerical predictions of the horseshoe vortex can be seen with different models. For other simulations, Escauriaza and Sotiropoulos (2011) developed a Lagrangian particle model in computation for a surface-mounted circular cylinder in order to reveal the mechanism of bed-load sediment transport in turbulent junction flows.

II. THE PROBLEM AND FORMULATION

Shown in Fig. 1 is the flat-plate boundary layer passing a wing of finite span. The wing is vertically mounted on the plate. The cross section of the wing is a combination of a semi-ellipse at the nose and a NACA0020 airfoil at the tail. They join at the location of maximum thickness. The ratio of the two axes is 3:2 and the major axis is aligned with the incoming flow. The maximum thickness of the wing is $T = 0.235c$ and the span of the wing is $s = 0.75c$, where c is the chord length of the wing.

In turbulent flows, if we decompose the velocity u_i and pressure p in time-averaged and fluctuating components,

$$u_i(x_i,t) = \overline{u}(x_i,t) + u'(x_i,t)$$
$$p(x_i,t) = \overline{p}(x_i,t) + p'(x_i,t) \tag{1}$$

where the quantities with bar are time-averaged components and the rest terms on the right hand side are fluctuating ones, and x_i and t denotes space coordinates and time, respectively, then the turbulent flow for the present problem can be modeled by the incompressible Reynolds-averaged Navier-Stokes (RANS) equations

$$\frac{\partial \overline{u}_i}{\partial x_i} = 0$$
$$\frac{\partial \overline{u}_i}{\partial t} + \overline{u}_j \frac{\partial \overline{u}_i}{\partial x_j} = -\frac{1}{\rho}\frac{\partial \overline{p}}{\partial x_i} + \frac{1}{\rho}\frac{\partial}{\partial x_j}\left(\tau_{ij} + \lambda_{ij}\right) \tag{2}$$

where ρ denotes the fluid density, τ_{ij} the viscous stress tensor evaluated in terms of the mean flow quantities, and λ_{ij} the Reynolds stress tensor. The viscous and Reynolds stress tensors can be expressed as

$$\tau_{ij} = \mu\left(\frac{\partial \overline{u}_i}{\partial x_j} + \frac{\partial \overline{u}_j}{\partial x_i}\right), \lambda_{ij} = -\rho\overline{u_i' u_j'} \tag{3}$$

where μ is the dynamic viscosity of fluid.

1. Turbulence Models

The Reynolds stresses incorporate the effects of the unresolved turbulent fluctuations on the mean flow. These apparent turbulent stresses significantly enhance momentum transport in the mean flow but they lead to six additional unknown quantities and, hence, the closure problem for the RANS equations. One way to cure this problem is the introduction of turbulence models in order to appropriately model the Reynolds stress. Various models have been proposed in the literature. Generally speaking, the turbulence models may be classified as eddy-viscosity models (based on Boussinesq approximation) and second moment models. The former includes zero-, one-, and two-equation models; the latter includes Reynolds-stress transport models.

In this study, six different turbulence models were employed. They cover the two categories of models. In the following, a brief comment for each of them will be first made. To shorten discussions in this sub-section, we omit all formulations which, nonetheless, are readily available in the references cited herein.

Five linear eddy-viscosity models were chosen in present study. The first one is the Spalart-Allmaras model, a one-equation model (Spalart and Allmaras, 1992). Typically, one-equation models include a viscosity-like variable as another equation. The Spalart-Allmaras model solves a transport equation for a modified eddy viscosity and the turbulent kinetic energy is not calculated. The formulation blends automatically from a viscous sub-layer formulation to a logarithmic formulation. It may be inaccurate for shear flow, separated flow, and decaying turbulence.

The rest three models belong to two-equation ones. Two-equation models account for history effects like convection and diffusion of turbulent kinetic energy. In this category, the standard k-ε model (Launder and Sharma, 1974) is most widely used in engineering applications. However, a wall function must be employed for this model. In their original intention, Launder and Sharma proposed it to improve the mixing-length model and to find an alternative to prescribing algebraically turbulent length scales in moderate to high complexity flows. Generally,

its performance is poor for flows with strong separation, large streamline curvature, and large pressure gradient.

The realizable k-ε model (Shih et al., 1995) is a variant of the standard one to improve simulations of flow with rotation, strong adverse pressure gradients, and mixing. It differs from the standard k-ε model in two ways. This model contains a new formulation for the turbulent viscosity and a new transport equation for the dissipation rate derived from an exact equation for the transport of the mean-square vorticity fluctuation. The term "realizable" implies that the model satisfies certain mathematical constraints on the Reynolds stresses, consistent with the physics of turbulent flows. However, this model may produce non-physical turbulent viscosity in situations with both rotating and stationary fluid zones.

The shear stress transport (SST) k-ω model (Menter, 1994) uses a blending function to gradually transition from the standard k-ω model near the wall to a high Reynolds number version of k-ε model in the outer portion of the boundary layer. In physics, the definition of the turbulent viscosity is modified to account for the transport of the principal turbulent shear stress. It is this feature that gives this model an advantage in terms of performance over both the standard k-ω model and the standard k-ε model. Nevertheless, it may overestimate turbulence in regions with large normal strain and converge slowly.

The last two models belong to the second-moment ones. The $V2$-f model (Laurence et al., 2004), similar to the standard k-ε version, is a nonlinear one. It incorporates some near-wall turbulence anisotropy as well as non-local pressure-strain effects. It is a general low-Reynolds-number turbulence model that is valid all the way up to solid walls, and therefore does not need to make use of wall functions. It can capture the features of attached or separated boundary layer flows.

The Reynolds stress model (Launder et al., 1975) is a higher-level elaborate turbulence model. Avoiding isotropic viscosity assumptions, it solves the individual Reynolds stresses directly, employing differential transport equations. The individual Reynolds stresses are then used to obtain closure of the Reynolds-averaged momentum equations. Unfortunately, several terms in the exact equation are unknown and modelling assumptions are required in order to close the equations. It can be used for highly swirling flows and stress-driven secondary flows.

2. Computational Strategy

In this study, ANSYS Fluent 15.0 was employed. Steady flows at zero angle of attack to the wing were computed with six available turbulence models. Due to flow symmetry, computations were conducted in a half flow domain. The SIMPLEC algorithm was adopted for iterations for the velocity and pressure fields. For more effective computations, we employed non-structured polyhedral grids in Fluent. It has been shown that this type of mesh considerably reduces mesh skewness (Lanzafame et al., 2013).

The computational domain extends 4.3c upstream from the leading edge of the wing, 6.9c downstream from the trailing edge, 4.3c in width, and 2.4c in the spanwise direction from the flat plate. The total number of grids is about 4.7×10^6. Fig. 2 shows the mesh near the wing and part of the refinement. To capture the vortex structure, we refined the local grid near the wing, the flat plate, and rear regions.

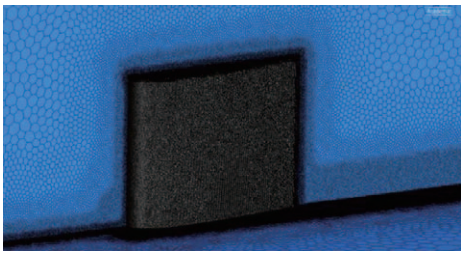

(a) Grid near the wing

(b) Local refinement near the wing section

Fig. 2. Grid for the present study.

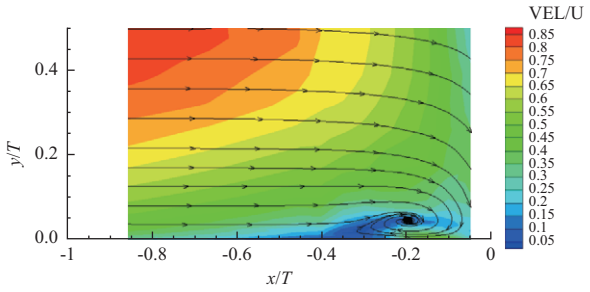

Fig. 3. Vortical flow structure (Devenport and Simpson, 1990).

III. SOME RESULTS AND DISCUSSIONS

The results presented in the following discussion were obtained at the Reynolds number $Re = 5 \times 10^5$, based on the chord length of the wing. The upstream velocity distribution was specified according to the report by Devenport and Simpson (Devenport and Simpson, 1990). And all comparisons of our results are made with data available in this report.

1. Vortical Flow on the Symmetric Plane

Shown in Fig. 3 are the streamlines of flow on the symmetric plane according to the LDA data by Devenport and Simposon (1990). It appears that only one vortex was revealed. Its center is approximately at $x/T = -0.2$. However, we have to keep in mind that the measurement region and the number of measurement points are quite limited. This may result in incapability of detailed flow field measurement, especially for those of smaller scales.

The vortex systems obtained with different turbulence models are shown in Fig. 4 in which the color plots exhibit the global picture and the black-and-white ones show the local details near the corner of junction at the leading edge. Furthermore,

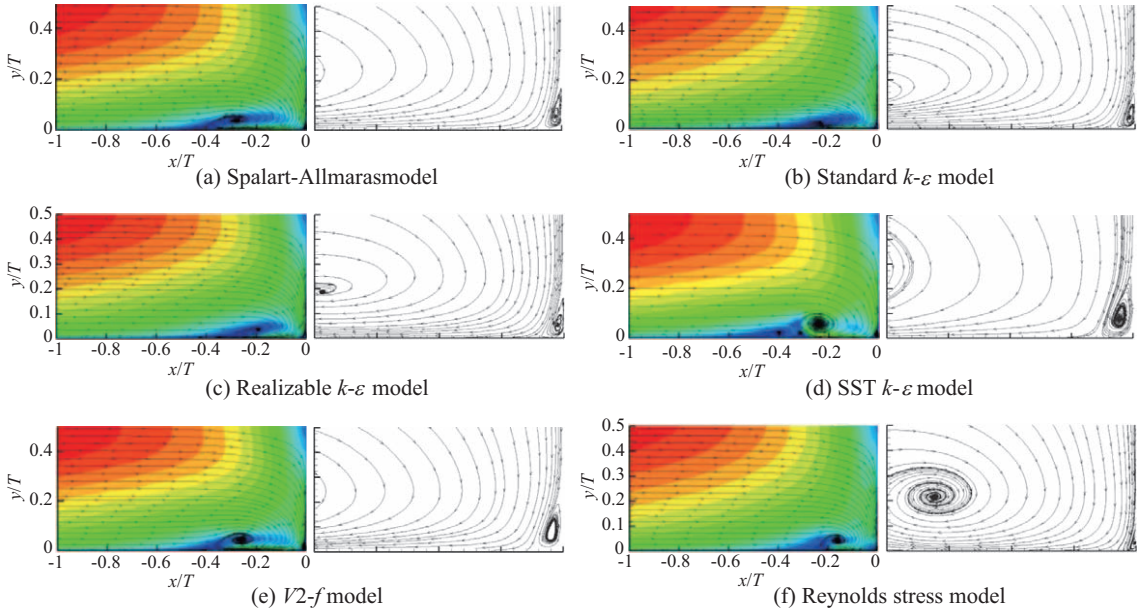

Fig. 4. Vortex system on the symmetrical plane (See Fig. 3 for color legend).

the color in each plot represents the velocity magnitude variation. The major vortex core position in x-direction varies from model to model. The result by the one-equation model differs most significantly from the experimental data; others are much closer. The SST k-ω model results in three vortices, though two of them are very small which might be beyond the capability of LDA measurement (Devenport and Simpson, 1990). A similar phenomenon is also observed with the omega Reynolds-stress model which is not presented here. Even though these two vortex systems are totally different, they are both possible in junction flows (Simpson, 2001).

In y-direction, the major vortex core position also varies from one model to another one. The experimental data (Devenport and Simpson, 1990) show that it is at about y/T = 0.05. The computational results show that the two nonlinear models best predicted the major vortex core position (y/T = 0.045 by the $V2$-f model and 0.044 by the Reynolds-stress model). The result by the standard k-ε model appears to be far more underestimated with y/T = 0.025 whereas the SST k-ω model over-predicted the position with y/T = 0.06. For the other two models, the predicted values are the same; i.e., y/T = 0.04.

As to the shape of the major vortex, the experimental data show that it is oblate. Most models also predicted a oblate shape; the only exception is the Reynolds-stress model which resulted in a big and round shape. The results by the Spalart-Allmaras model and the $V2$-f model best agree with the experimental one. However, the former one has the worst prediction on the location of the vortex.

In addition, a corner vortex appears in all models. This is not detected in the experiment by Devenport and Simpson (1990) which might be due to the limitation on measurement region because the nearest measurement point is 0.05T away from the leading edge of the wing. The separation point is at around x/T = 0.025 for the Spalart-Allmaras, standard k-ε, and Reynolds-stress models, 0.03 for realizable k-ε and $V2$-f models, and 0.04 for SST k-ω model, compared to the experimental value of 0.025 (Devenport and Simpson, 1989). It is also the attachment point of the separated flow more upstream of the wing. As a simple summary, we found that there is a 4-vortex system for the SST k-ω model. For other models, what we got is a 2-vortex system.

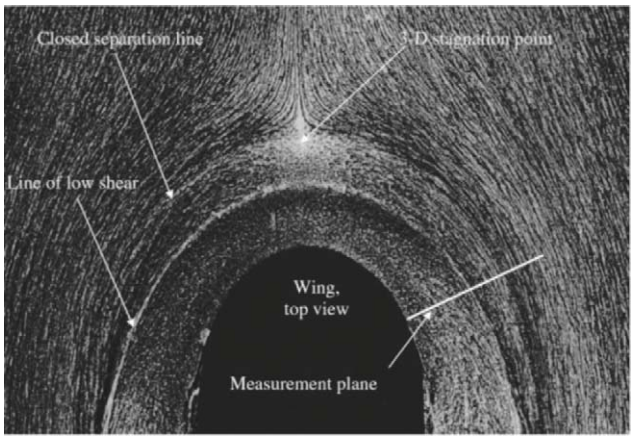

Fig. 5. Oil flow visualization (Ölçmen and Simpson, 2006).

2. Flow Structure Near the Leading Edge

Fig. 5 shows the oil film visualization (Ölçmen and Simpson, 2006). The flow separates at about x/T = -0.47 (Devenport and Simpson, 1989). A closed separation line originating from this point extends symmetrically downstream on both sides of the wing. In addition, a line of low mean shear stress which is between the wing and the separation line is also apparent. This line intersects the symmetric plane at about x/T = -0.28.

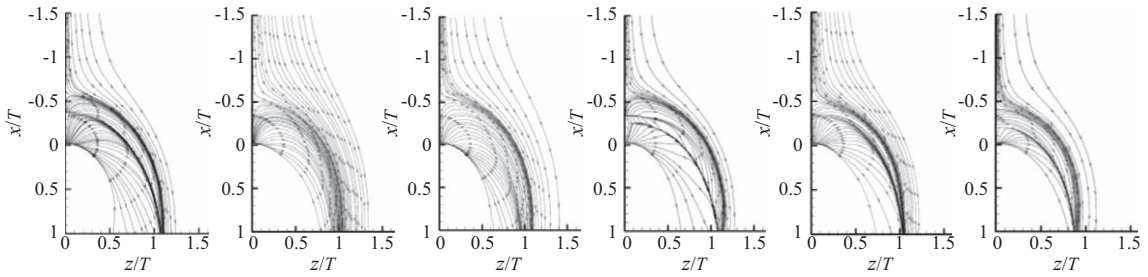

(a) Spalart-Allmaras (b) Standard k-ε (c) Realizable k-ε (d) SST k-ε (e) $V2$-f (f) Reynolds stress

Fig. 6. Limiting streamline patterns on the flat plate for different turbulence models.

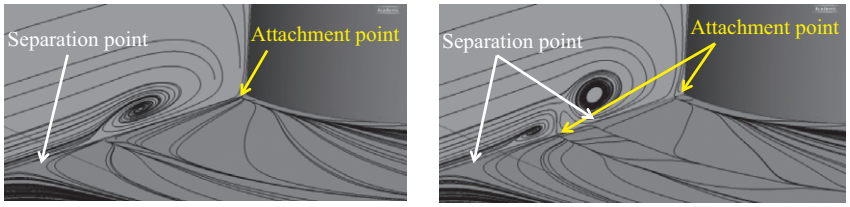

(a) Two-vortex system (b) Four-vortex system

Fig. 7. Limiting streamline topology.

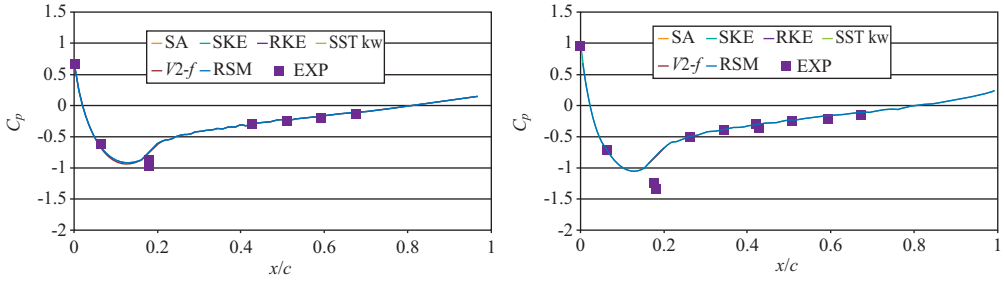

(a) $y/T = 0.13279$ (b) $y/T = 0.39837$

Fig. 8. Pressure distributions on the wing surface.

Fig. 6 shows the limiting streamlines (or skin friction lines). Several physical phenomena can be observed in these plots. First of all, the main flow separation point can be identified. For most models, the position of the separation point does not vary significantly. They are at about x/T = -0.5, quite consistent with the experimental data. The only exception is the one by the Spalart-Allmaras model in which the flow separates at about x/T = -0.6. In addition, the developments of the separation line for different models are comparable. Experimental data shows that the line crosses x/T = 1 at about z/T = 1.0. In our computations, the value of z/T varies from about 0.9 for the Reynolds stress model to 1.1 for the Spalart-Allmaras and realizable k-ε models. Furthermore, the separation point near the corner can be clearly observable for all models in Fig. 6.

In additional to these separation and attachment points, we can also find other similar points in some of the plots. We pointed out above that SST k-ω model resulted in a 4-vortex system and others a 2-vortex system. Therefore, we can expect that the limiting streamline structure for the SST k-ω model must be more complicated. It has another separation and reattachement points as shown in Fig. 6(d). As to the 2-vortex system, we find another separation point in Figs. 6(a), (e), and (f.). However, the two k-ε models do not reveal this feature if we observe Figs. 6(b) and (c). Fig. 7 shows the limiting streamline topology for both 4- and 2-vortex systems. From these two plots, we can clearly identify the separation points. Nevertheless, the flow pattern in Fig. 5 seems to imply that the flow structure should be a 2-vortex system. Of course, the present study focuses on steady flow. Such mean vortex patterns are not representative of the highly unsteady instantaneous flow.

Furthermore, the line of low shear can be clearly observed in Figs. 6(a), (d), (e), and (f). However, for the Spalart-Allmaras and $V2$-f models, the predicted location on the symmetric plane is upstream of the location in experiments. For the other two models, the prediction is much closer to the experimental data. Of course, the structure in Fig. 6(f) is even closer to that revealed in the experiment.

3. Pressure Distributions

Fig. 8 presents the pressure distributions on the wing sur-

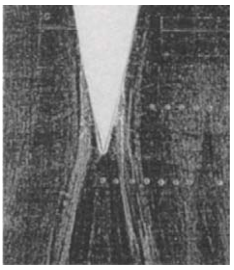

Fig. 9. Flow visualization at the trailing edge (Simpson, 2001).

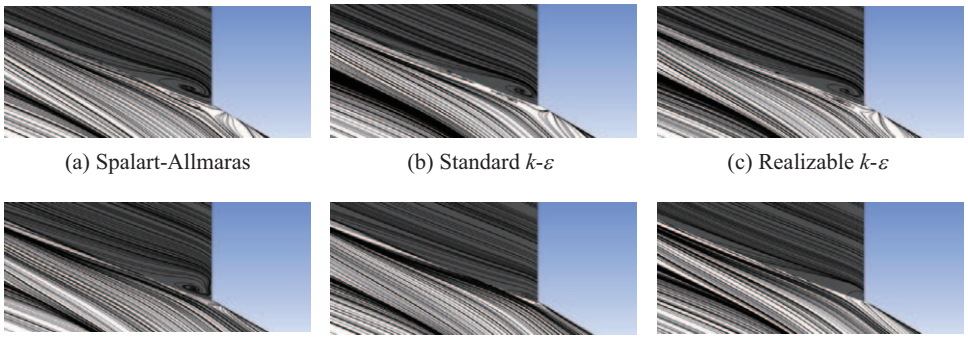

Fig. 10. Separation near the trailing edge of the wing.

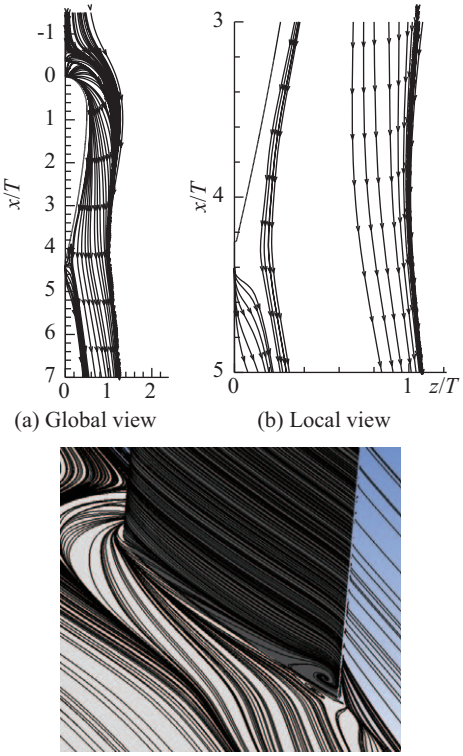

Fig. 11. Overall flow pattern around the wing.

face at $y/T = 0.13279$ and 0.39837. It is found that the pressure distributions for all six models coincide with each other and their differences are almost indistinguishable. Compared to the experimental data, the pressure prediction at $y/T = 0.13279$ is better than that at $y/T = 0.39837$. We also compare the data on the wing at different heights and find that near $x/c = 0.2$, there is a significant discrepancy between the computational results and the experimental data. This could be because, near this point which is close to the point of maximum thickness ($x/c = 0.18$), the blockage effect in wind tunnel experiments might be more significant, the value of pressure coefficient precipitously drops and rises and is difficult to be accurately predicted by these six models.

4. Flow Structure near the Trailing Edge

Fig. 9 shows the surface oil flow visualization of the junction flow in the trailing edge region of the wing (Simpson, 2001). It appears that the flow separates near the trailing edge. The limiting streamlines of the computed solutions in the local area are shown in Fig. 10. At a glance, we may find that not all solutions reveal such a flow structure. The results show that the linear models have a better capability to capture the flow separation than the nonlinear ones. The four linear models lead to similar separation. Nevertheless, the flow separation by the *V2-f* model was barely captured very near the trailing edge and not found in the solution by the Reynolds stress model. It is quite interesting to find that the nonlinear high-order methods are not more capable of resolving such a flow phenomenon in a very small region.

Fig. 11 shows the overall picture of limiting streamlines in the region where the wing is located. The results used in this plot

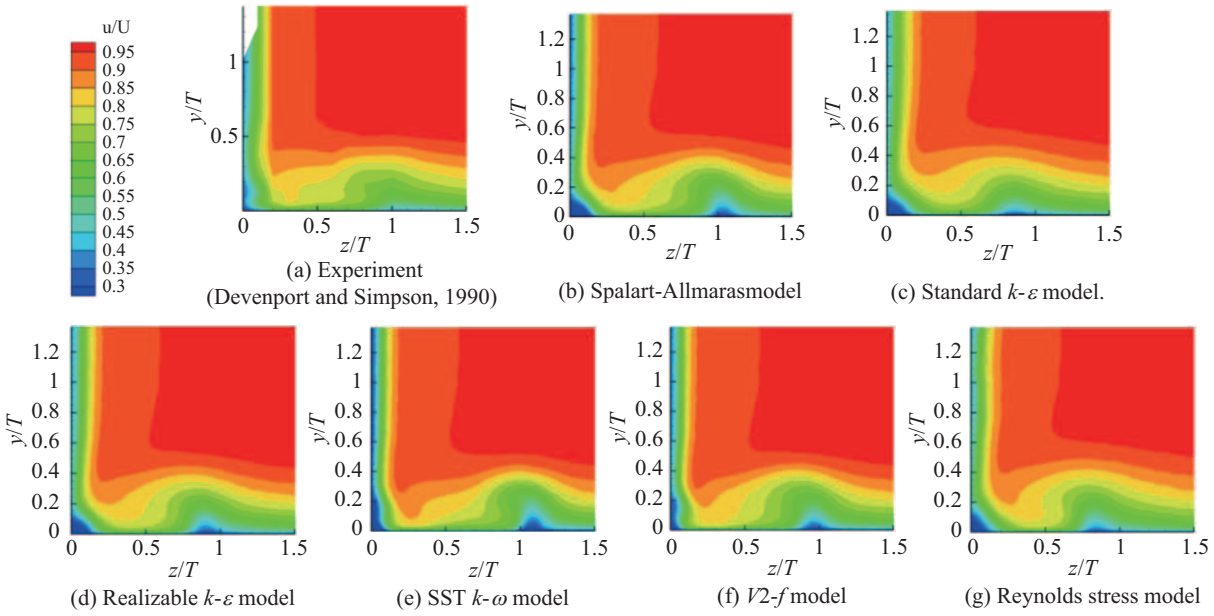

Fig. 12. Wake distribution on the plane of x/c = 1.05.

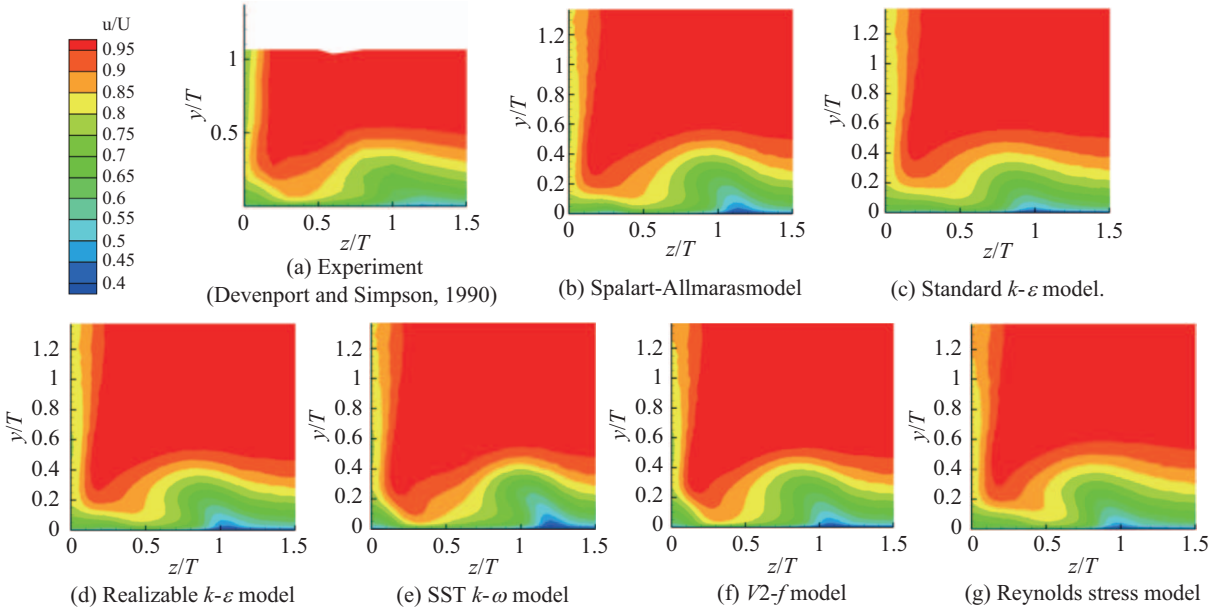

Fig. 13. Wake distribution on the plane of x/c = 1.50.

are those obtained by the Spalart-Allmaras model. Compared to the fishtail like separation shown in Fig. 9, this model successfully captures the flow phenomenon. We also find that the fishtail like separation is also clearly shown for the other three linear models, but not for the two nonlinear models. The three-dimensional plot shown in Fig. 11(c) clearly depicts the three-dimensional flow separation which appears on both the wing and the flat plate surfaces. Similar results were obtained for the rest of three linear turbulence models.

5. Wake Structures

The wake distributions at x/c = 1.05 and 1.50 are discussed. They are shown in Figs. 12 and 13.

At x/c = 1.05, we find that, at the first glance, the wake seems underestimated in the corner region near the symmetric plane for most models when comparing with the experimental data (Devenport and Simpson, 1990). The result by the $V2$-f model appears to be the only exception and, hence, agrees much well with the LDA data (Devenport and Simpson, 1990). However, we should also point out that the available LDA data is quite sparse and the wake distribution is more qualitative than quantitative in the corner region. If we refer to Fig. 10, we can see

that the wake region is bigger for the models which result in flow separation near the leading edge. Again, the only exception is the result by the *V*2-*f* model in which no separation is induced. Even though in the experiment the flow separates, it appears that the low-speed wake region is restricted to a very small region. In addition, there appears another low-speed region at about $z/T = 1.0$. It is more significant for some models. The computations show that this region begins to develop at the cross section where the maximum thickness of wing takes place. It grows downstream before the flow reaches the trailing edge. After passing the trailing edge, it shrinks very rapidly. Furthermore, it decays further downstream and drifts away from the symmetric plane, as shown in Fig. 13. Nevertheless, it appears that such a slow-speed region is not observed in the experimental data.

At $x/c = 1.5$, the low-speed wake region disappears. It seems to imply that the turbulent mixing is efficient and the flow becomes much more uniform. The wake distributions obtained from different turbulence models are similar and close to the one obtained in experiment, except for the low-speed region at about $z/T = 1$. Again this region is not captured in the experiment. Nevertheless, speed is raised, compared to that at $x/c = 1.05$.

IV. CONCLUSIONS

In this study, we have investigated some features of junction flows by computations with different turbulence models. Only steady flow is considered in the present study. Various flow structures and physical quantities were studied. The results show that the choice of turbulence model may have strong influence on the revelation of flow structure. While some can reasonably predicted the flow, others may lead to quite different flow structures.

For the vortical flow structure, the SST k-ω model leads to a 4-vortex system on the symmetric plane while the other models result in a 2-vortex system. Nevertheless, the two kinds of flow structures are possible in junction flows (Simpson, 2001) though the experiment data to which we compared our results seems to exhibit the 2-vortex system. All models capture the tiny vortex in the corner of the juncture at wing leading edge though its size strongly depends on the selected model.

The location of the separation point position is reasonably predicted, compared to the experimental data. The development of the separation lines with different models also agree well with each other. However, the low shear line seems not well predicted, especially for two k-ε models.

The pressure distribution can be accurately predicted with various turbulence models, except in the region of rapid variation.

The linear models can predict more accurately the tiny three-dimensional separation near the trailing edge. In this respect, the nonlinear ones are not as capable. Nevertheless, the flow development in the near wake region at $x/c = 1.05$ is strongly affected by the separation. It appears that the flow dissipation exhibited in the computed results is not so efficient that the low-velocity region is much more significant, compared to the experiment data.

Generally speaking, there is no single model which can well predict all physical phenomena. Even the nonlinear models cannot predict certain flow physics more accurately than the linear ones.

REFERENCES

Apsley, D. D. and M. A. Leschziner (2001). Investigation of advanced turbulence models for the flow in a generic wing-body junction. Flow, Turbulence and Combustion 67, 22-55.

Baker, C. J. (1979). The laminar horseshoe vortex. Journal of Fluid Mechanics, 95, 347-367.

Deng, G. B. and J. Piguet (1992). Navier-Stokes computations of horseshoe vortex flow. International Journal for Numerical Methods in Fluids 15, 99-124.

Devenport, W. J. and R. L. Simpson (1989). Time-dependent structure in wing-body junction flows. Turbulent Shear Flows 6 (edited by J.-C. Andre, J. Cousteix, F. Durst, B. Launder, F.W. Schmidt, and J.H. Whitelaw), Springer, Berlin, 232-248.

Devenport, W. J. and R. L. Simpson (1990). An experimental investigation of the flow past an idealized wing-body junction: final report. Virginia Polytechnic Institute and State University, Report VPI-AOE-172.

Dickinson, S. C. (1986a). An experimental investigation of appendage-flat plate junction flow. Volume 1. Description, Final Report Naval Ship Research and Development Center, Bethesda, MD.

Dickinson, S. C. (1986b). An experimental investigation of appendage-flat plate junction flow. Volume 2. Elliptical nose appendage data base, Final Report Naval Ship Research and Development Center, Bethesda, MD.

Escauriaza, C. and F. Sotiropoulos (2011). Lagrangian model of bed-load transport in turbulent junction flows. Journal of Fluid Mechanics, 666, 36-76.

Fleming, J. L., R. L. Simpson, J. E. Cowing and W. J. Devenport (1993). An experimental study of a turbulent wing-body junction and wake flow. Experiments in Fluids 14, 366-378.

Fu, S., Z. Xiao, H. Chen, Y. Zhang and J. Huang (2007). Simulation of wing-body junction flows with hybrid RANS/LES methods. International Journal of Heat and Fluid Flow 28, 1379-1390.

Lanzafame, R., S. Mauro and M. Messina (2013). Wind turbine CFD modeling using a correlation-based transitional model. Renewable Energy 52, 31-39.

Launder, B. E., G. J. Reece and W. Rodi (1975). Progress in the development of a Reynolds-stress turbulent closure. Journal of Fluid Mechanics 68, 537-566.

Launder, B. E. and B. I. Sharma (1974). Application of the energy dissipation model of turbulence to the calculation of flow near a spinning disc. Letters in Heat and Mass Transfer 1, 131-138.

Laurence, D. R., J. C. Uribe and S. V. Utyuzhnikov (2004). A robust formulation of the v2-f model. Flow Turbulence and Combustion 73, 169-185.

Menter, F. R. (1994). Two-equation eddy-viscosity turbulence models for engineering applications. AIAA Journal 32, 1598-1605.

Ölçmen, S. M. and R. L. Simpson (2006). Some features of a turbulent wing-body junction vortical flow. International Journal of Heat and Fluid Flow 27, 980-993.

Pierce, F. J. and J. Shin (1992). The development of a turbulent junction vortex system (data bank contribution). Journal of Fluids Engineering 114, 559-565.

Shih, T. H., W. W. Liou, A. Shabbir, Z. Yang and J. Zhu (1995). A new k-ε eddy viscosity model for high Reynolds number turbulent flows-model development and validation. Computers and Fluids 24, 227-238.

Simpson, R. L. (2001). Junction flows. Annual Review of Fluid Mechanics 33, 415-443.

Spalart, P. R. and S. R. Allmaras (1992). A one-equation turbulence model for aerodynamic flows. AIAA Paper 92-0439.

Wong, J. H. and E. K. Png (2009). Numerical investigation of the wing-body junction vortex using various large eddy simulation models. 39th AIAA Fluid Dynamics Conference, San Antonio, TX, USA.